



Geological Survey of Canada

CURRENT RESEARCH  
2003-C15

**Deformation history and metamorphism  
of a synformal depression, Longstaff  
Bluff Formation metaturbidite,  
central Baffin Island, Nunavut**

*M.M. Allan and D.R.M. Pattison*

2003



Natural Resources  
Canada

Ressources naturelles  
Canada

Canada

CURRENT RESEARCH

©Her Majesty the Queen in Right of Canada 2003  
ISSN 1701-4387  
Catalogue No. M44-2003/C15E-IN  
ISBN 0-662-33537-6

A copy of this publication is also available for reference by depository libraries across Canada through access to the Depository Services Program's website at <http://dsp-psd.pwgsc.gc.ca>

A free digital download of this publication is available from the Geological Survey of Canada Bookstore web site:

<http://gsc.nrcan.gc.ca/bookstore/>

Click on Free Download.

**All requests for permission to reproduce this work, in whole or in part, for purposes of commercial use, resale, or redistribution shall be addressed to: Earth Sciences Sector Information Division, Room 402, 601 Booth Street, Ottawa, Ontario K1A 0E8.**

### **Authors' addresses**

***M.M. Allan*** ([mmallan@earth.leeds.ac.uk](mailto:mmallan@earth.leeds.ac.uk))  
*School of Earth Sciences  
University of Leeds  
Leeds LS2 9JT, United Kingdom*

***D.R.M. Pattison*** ([pattison@geo.ucalgary.ca](mailto:pattison@geo.ucalgary.ca))  
*Department of Geology and Geophysics  
University of Calgary  
2500 University Drive NW  
Calgary, Alberta T2N 1N4*

Publication approved by Continental Geoscience Division

# Deformation history and metamorphism of a synformal depression, Longstaff Bluff Formation metaturbidite, central Baffin Island, Nunavut

M.M. Allan and D.R.M. Pattison

*Allan, M.M. and Pattison, D.R.M., 2003: Deformation history and metamorphism of a synformal depression, Longstaff Bluff Formation metaturbidite, central Baffin Island, Nunavut; Geological Survey of Canada, Current Research 2003-C15, 11 p.*

---

**Abstract:** A metamorphism-deformation history has been reconstructed for a small area of poly-deformed metaturbidite of the Longstaff Bluff Formation on the northern margin of the Foxe Fold Belt, central Baffin Island. The area studied is an elongate synformal depression with main fold features related to the ca. 1.8 Ga Trans-Hudson Orogen. Pelite and semipelite contain low-pressure cordierite±andalusite assemblages. Field and microstructural relationships document four tectonic events, constrained with respect to metamorphic mineral growth events. Cordierite and prismatic andalusite growth (550–580°C, 3–3.5 kbar) postdates a weak early fabric ( $S_1$ ) and predates the development of a regionally penetrative, north-dipping fabric ( $S_2$ ) related to orogen-parallel folding ( $D_2$ ). Late interstitial andalusite growth (580–600°C, 3.5–4.0 kbar) postdates  $D_2$  and represents peak metamorphism. Late, locally developed crenulation cleavages record one approximately orogen-parallel event ( $D_3$ ) unrelated to any regional structures and a second event ( $D_4$ ) that may be related to late north-trending regional crossfolding.

**Résumé :** L'évolution du métamorphisme et de la déformation a été reconstituée en ce qui concerne un petit secteur de métaturbidites polydéformées de la Formation de Longstaff Bluff situé à la marge septentrionale de la zone de plissement de Foxe, dans la partie centrale de l'île de Baffin. La région étudiée est une dépression synforme allongée dont les principales entités plissées sont liées à l'orogène trans-hudsonien remontant à 1,8 Ga. Des pélites et des semi-pélites renferment des associations à cordiérite±andalusite formées dans des conditions de faible pression. Des liens établis par des observations sur le terrain et l'examen de microstructures révèlent quatre épisodes tectoniques, chacun d'eux étant encadré par des épisodes de croissance de minéraux métamorphiques. La croissance de cristaux de cordiérite et d'andalusite prismatique (550 à 580°C, 3 à 3,5 kbar) est postérieure à une fabrique ( $S_1$ ) peu marquée de formation précoce et antérieure à l'apparition d'une fabrique pénétrative ( $S_2$ ) de pendage nord d'étendue régionale, qui est liée à un plissement ( $D_2$ ) parallèle à l'axe de l'orogène. La croissance tardive de cristaux interstitiels d'andalusite (580 à 600°C, 3,5 à 4,0 kbar) est postérieure à  $D_2$  et correspond à l'atteinte des conditions maximales du métamorphisme. La présence, par endroits, d'un clivage de crénulation d'apparition tardive révèle un épisode de déformation ( $D_3$ ), dont les effets se sont fait sentir plus ou moins parallèlement à l'axe de l'orogène, mais auquel aucune structure d'étendue régionale n'est associée, et un deuxième épisode ( $D_4$ ), qui pourrait être lié à la formation tardive de plis transverses d'orientation nord-sud à l'échelle régionale.

## INTRODUCTION

Central Baffin Island encompasses the northern margin of the Paleoproterozoic Trans-Hudson Orogen (Hoffman, 1988), a collisional belt suturing the Rae–Hearne Province to the north, and the Superior Province to the south. This structural region, known as the ‘Foxe Fold Belt’, has been mapped at reconnaissance scale and later in selective detail (Corrigan et al., 2001; Scott et al., 2002; Wodicka et al., 2002, and references therein). The Central Baffin Project, the latest stage of bedrock mapping along this segment of the Trans-Hudson Orogen, was launched as a multidisciplinary partnership of the GSC, the Canada-Nunavut Geoscience Office, and the Polar Continental Shelf Project during the 2000–2002 field seasons. From north to south, this map area brackets Archean basement granitoid rocks of the Rae Province, the

Paleoproterozoic Piling Group supracrustal sequence, and the 1.87 to 1.84 Ga Cumberland Batholith (Wodicka et al., 2002) and related plutonic rocks (Fig. 1).

Regional structural and metamorphic features are summarized in Corrigan et al. (2001), St-Onge et al. (2001a, b, c, d, 2002a, b, c), and Scott et al. (2002). A detailed interpretation of regional structures is the subject of a current M.Sc. thesis (F. Berniolles, Queen’s University). Regional metamorphism and its causes are being addressed in a current Ph.D. thesis (K. Dubach, Queen’s University). This investigation provides a link between the two above-mentioned studies by focusing on the relationship between metamorphism and deformation. This relationship was examined in a small study area south of Flint Lake, in metaturbidite of the Upper Piling Group (Fig. 1 and 2). Microtextures and mineral assemblages, combined with thermodynamically calculated phase

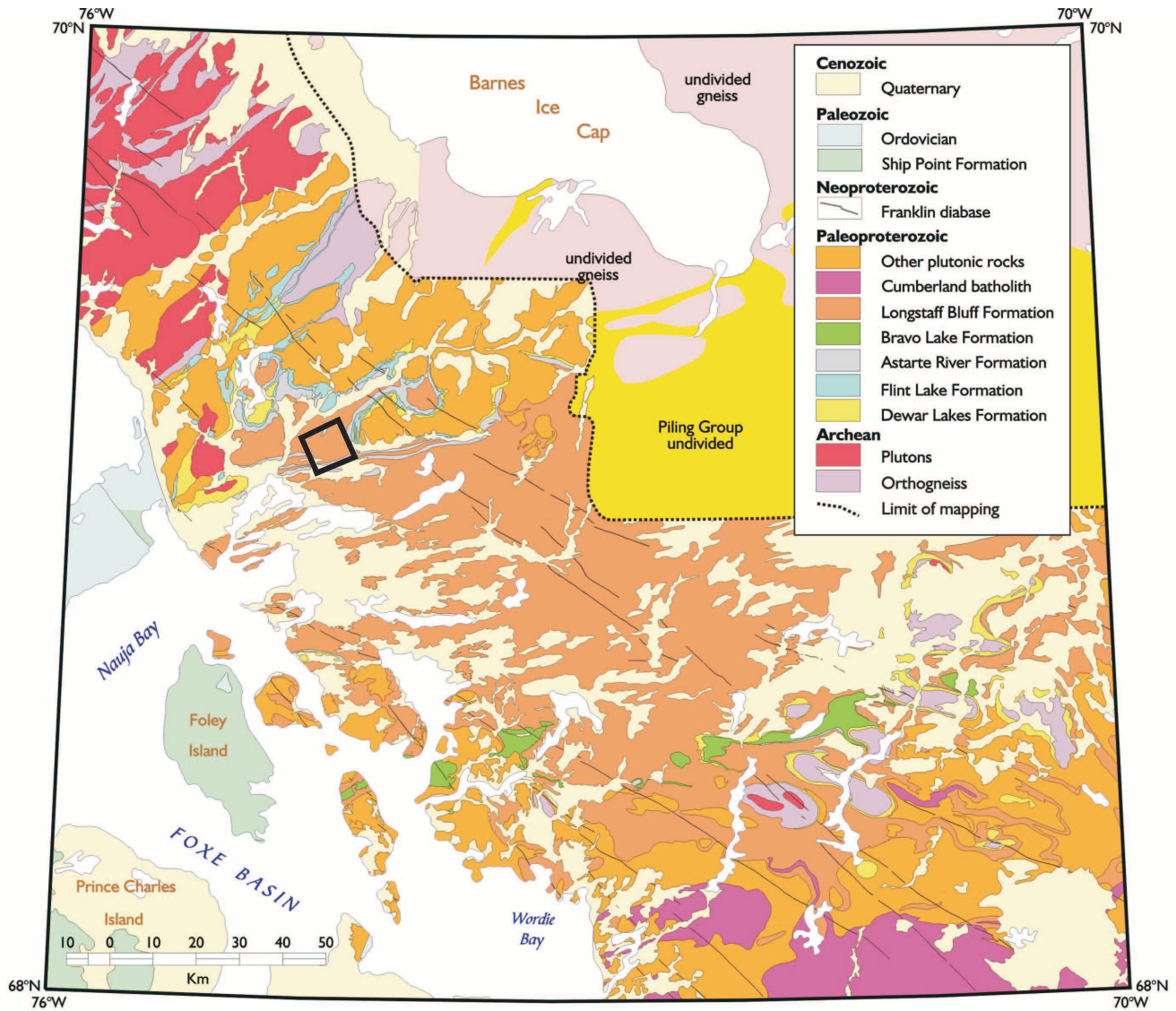


**Figure 1.** Bedrock geology of the Central Baffin Project area, not including areas mapped in the 2002 field season. The black box outlines the study area in Figure 2 (after St-Onge et al., 2002a, Fig. 2).

equilibria and quantitative electron microprobe analyses, have been used to establish a pressure-temperature-deformation-time model for the study area. An attempt is made to apply these interpretations to regional tectonic and metamorphic events recorded by units of the Piling Group.

## **GEOLOGICAL SETTING**

The supracrustal Piling Group overlies ca. 2.8 Ga plutonic rocks of the Rae Province (Wodicka et al., 2002). From oldest to youngest, the Piling Group comprises the Dewar Lakes Formation (dominantly quartzite), the Flint Lake Formation (carbonate rock), the Astarte River Formation (sulphidic schist and iron-formation), and the Longstaff Bluff Formation (psammitic to pelitic metaturbidite). This last formation is the thickest unit in the Piling Group (Fig. 1). Rocks in the study area are cordierite±andalusite schist of the Longstaff Bluff Formation.

## **STRUCTURAL SETTING**

The Piling Group stratigraphy is affected by three main regional deformation events (e.g. Corrigan et al., 2001; Scott et al., 2002). A Paleoproterozoic thin-skinned deformation event ( $D_{1p}$ ) is reflected in low-angle structural repetitions of the lower Piling Group stratigraphy, isoclinal folding in the Dewar Lakes Formation, and fold-limb truncations in the Longstaff Bluff Formation. A subsequent  $D_{2p}$  event resulted in  $F_{2p}$  folding of both cover stratigraphy and plutonic basement. These folds trend approximately east-northeast (orogen-parallel) and are open to isoclinal and dominantly upright. A later crossfolding event ( $D_{3p}$ ) trending approximately north-south resulted in long-wavelength, open  $F_{3p}$  folding. The interference of  $F_{3p}$  with  $F_{2p}$  resulted in dome-and-basin fold morphology, responsible for the exposure of a series of gneiss-cored domes, interpreted to be ca. 2.8 Ga Rae Province basement (Wodicka et al., 2002; Fig. 1).

The structural style of the study area is also related to  $F_{2p}$ – $F_{3p}$  fold interference. The dominant fold structure is an open syncline striking west-southwest, with an axial plane dipping steeply north-northwest (Fig. 2), which is related to orogen-parallel  $F_{2p}$  folding observed regionally throughout the Piling Group (St-Onge et al., 2001a, b, c, d, 2002a, b, c). Superimposed on this syncline is a broad, open, long-wavelength syncline with an approximately north-trending fold axis, related to  $D_{3p}$ . The resultant structure is an elongate syn-formal depression with its long axis oriented east-northeast (Fig. 2).

## **METAMORPHIC SETTING**

Piling Group sedimentary rocks show a range of metamorphic grade from greenschist to lower granulite facies. Diagnostic mineral assemblages are most commonly found in semipelitic and pelitic beds of the Longstaff Bluff Formation, exposed over most of the Central Baffin Project map area

(Fig. 1). Lowest metamorphic grades occur near the centre of this map area (Fig. 1). Metamorphic grade increases to the north, south, and east. The pelitic assemblages used to define metamorphic zones are biotite+muscovite±chlorite, biotite+muscovite+cordierite±andalusite, sillimanite+K-feldspar+leucosome, and garnet+cordierite+K-feldspar+leucosome. This sequence of metamorphic zones represents pressures of 2.5 to 4 kbar (cf. facies series 2a, Pattison and Tracy, 1991). The rocks in the study area comprise biotite+muscovite-bearing psammite and porphyroblastic muscovite+biotite+cordierite±andalusite schist, with no apparent variation in grade across the study area.

## **FIELD RELATIONSHIPS**

Massive psammite (beds up to 2 m) is dominant in the study area, although graded beds containing psammitic, semipelitic, and rare pelitic layers occur (Fig. 3). Reverse metamorphic grading is observed in the form of increasing cordierite and andalusite porphyroblast abundance toward the pelitic tops of graded beds. Low-angle crossbedding is rarely observed. Minor calcsilicate pods containing hornblende±garnet assemblages also occur and have been interpreted as metamorphosed carbonate concretions (Corrigan et al., 2001; Scott et al., 2002).

Cordierite is found in the semipelitic and pelitic zones of graded beds, as ellipsoidal porphyroblasts 2 to 10 mm long with randomly oriented to weakly aligned long axes. Egg-shaped cordierite porphyroblasts are wrapped by the muscovite+biotite-rich matrix fabric. In most rocks, cordierite has been largely pseudomorphed by shimmery aggregates of phyllosilicates (usually muscovite+chlorite). Andalusite is rarer, occurring only in the pelitic tops of some graded beds as blocky, equidimensional (5–10 mm), pinkish-grey porphyroblasts, commonly showing well exposed cleavage surfaces. Andalusite also occurs in a variety of more cryptic microscopic morphologies and is described in the next section.

Rocks in the field area have a dominant, north-northwest-dipping schistosity with an approximate mid-range value of  $260^{\circ}/40^{\circ}W$ . This orientation is consistent with fabric measurements made throughout the Central Baffin Project area. However, schistosity measurements do show considerable dip variation, most likely a function of cleavage refraction across psammite–pelite boundaries. Some east-west divergence of original fabric orientations is expected from  $F_{3p}$  crossfolding, yet none was observed, perhaps because the pre-existing dominant fabric dips steeply and  $F_{3p}$  is a low-amplitude, long-wavelength feature. Penetrative fabric development related to  $F_{3p}$  was not observed.

Rare muscovite-rich pelite in the core of the dominant east-northeast fold contains two intersecting sets of crenulations. A crenulation cleavage dipping steeply south clearly overprints the dominant, north-northwest-dipping foliation, but cannot be correlated with any fold features. A later set of crenulations, with wavelength similar to that of the

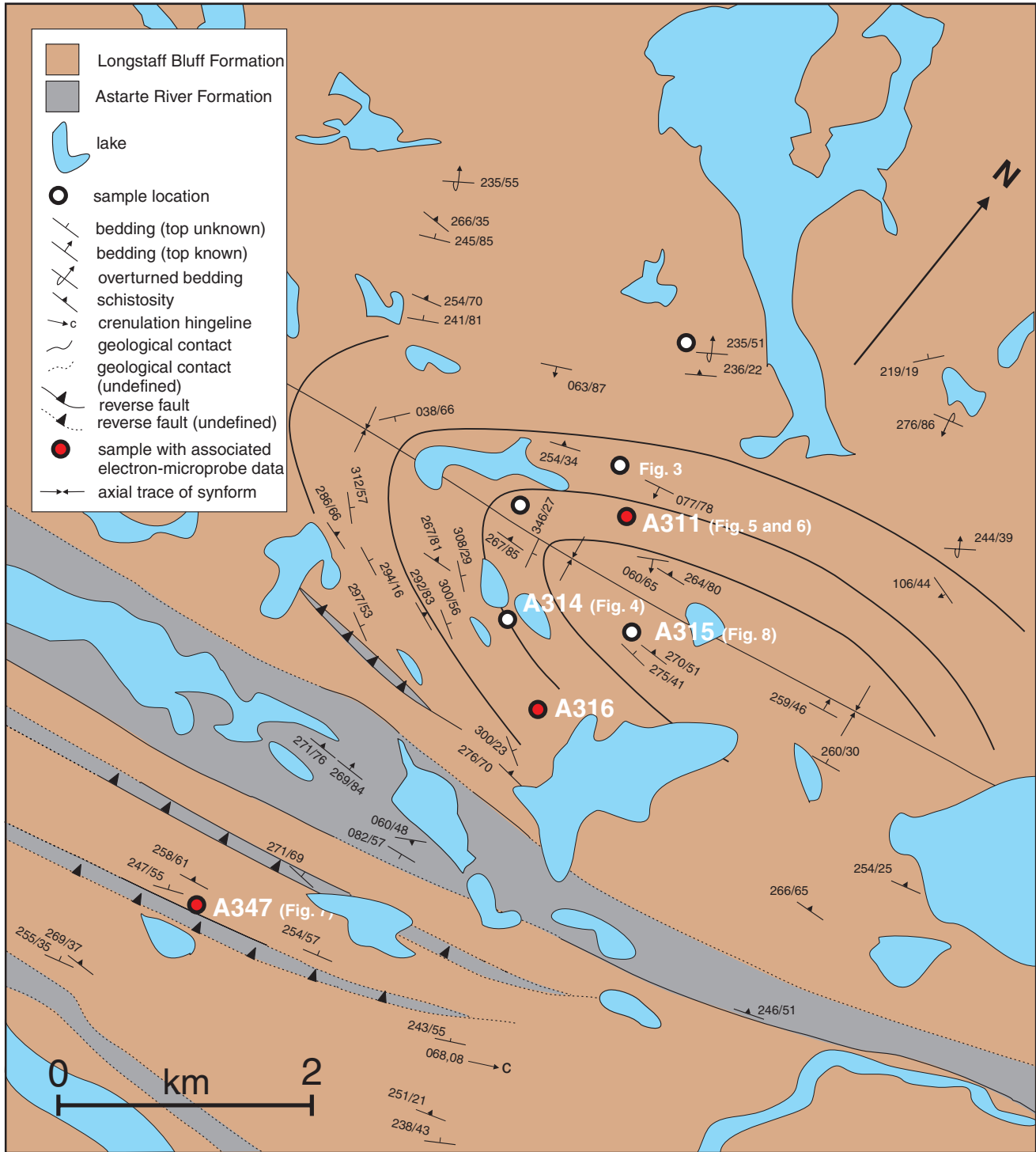


**Figure 2.** Simplified bedrock geology and representative structural measurements of the study area. Bedding-form lines, indicated in black, outline a synformal depression in metaturbidite of the Longstaff Bluff Formation. Structural repetitions of the Astarte River Formation are observed in the southern portion of the map area.



**Figure 3.** Graded beds within the Longstaff Bluff Formation, stratigraphic tops to left. Psammitic portions of the beds are grey; pelitic tops are brown. The hammer is 35 cm long.

first (1–2 mm), has north-plunging crenulation axes and therefore intersects the first set at a high angle (as measured on the north-northwest foliation plane).

## SAMPLING

Eight samples of semipelite and pelite were collected for microstructural analysis from both limbs and the hinge zone of the western portion of the dominant fold structure (Fig. 2). Samples were chosen to incorporate the maximum porphyroblast abundance, generally from the aluminous tops of graded beds. All samples contain cordierite and five contain andalusite. All samples were orientated in their original outcrop position. Two oriented thin sections were prepared from each sample so as to provide complementary views of microtextural features — one parallel to strike and 90° to schistosity, the other perpendicular to strike and 90° to schistosity, therefore lying in a vertical plane.

## PETROGRAPHY AND MICROTTEXTURAL ANALYSIS

Although the regional structural framework of Corrigan et al. (2001) has been used to interpret the main fold and fabric features in the study area (*see above*), the following discussion of microfabrics and their relative chronology is based entirely on the study area. Fabrics and deformation events are herein labelled  $S_1$  to  $S_4$  and  $D_1$  to  $D_4$ , respectively. An attempt is made to relate these to the regional deformation events.

All samples from the study area have a penetrative schistose fabric, here defined as  $S_2$ , striking approximately west-southwest, with varied northward dips. This schistosity is defined by the alignment of biotite+muscovite±chlorite in the matrix. This fabric envelopes ellipsoidal cordierite porphyroblasts, typically resulting in a muscovite-rich strain cap and a quartzose strain shadow (terminology *after* Passchier and Trouw, 1996; Fig. 4).

In seven of eight samples, cordierite has been altered to coarse aggregates of muscovite+chlorite±biotite, obscuring pre-alteration microtextures (Fig. 4). One sample (A311, Fig. 2) contains unaltered cordierite grains, which contain inclusions of large, randomly orientated biotite grains, in addition to inclusion trails of fine-grained quartz that define a weak planar fabric ( $S_1$ ; Fig. 5). This is the earliest recognizable

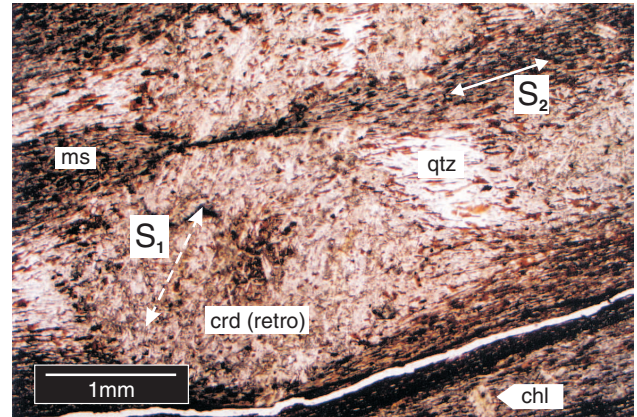


**Figure 4.** Sample A314, plane-polarized light. Retrogressed cordierite (crd) porphyroblasts show external fabric ( $S_2$ ) deflections and a coarse internal fabric arising from mimetic enhancement of a previous internal schistosity ( $S_1$ ). Note the muscovite-rich (ms) strain caps and quartz-rich (qtz) strain shadows. Chlorite (chl) occurs as microporphyroblasts overgrowing the  $S_2$  fabric.

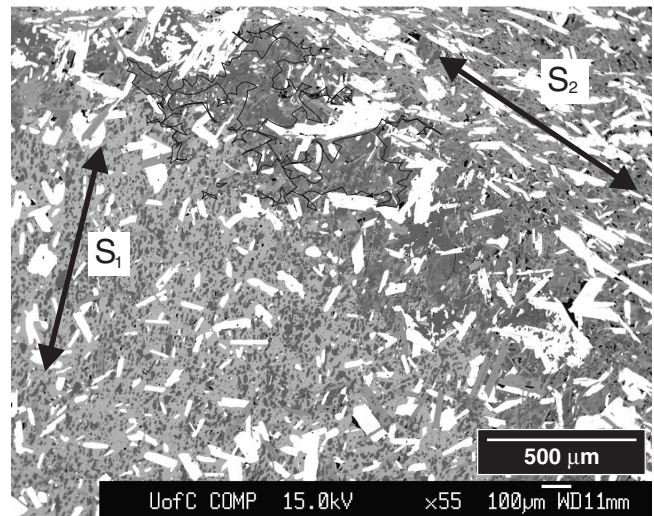


**Figure 5.** Backscattered electron image of the margin of an unaltered cordierite specimen (sample A311), showing randomly oriented biotite inclusions and fine-grained quartz inclusion trails, the latter defining the early  $S_1$  fabric. The internal schistosity ( $S_1$ ) lies at a high angle to, and abuts against, the external fabric ( $S_2$ ) defined by the alignment of biotite and muscovite. The dark band along the margin of the cordierite grain is a zone of pinitization.

fabric in the study area. In altered samples, a core of yellowish-brown, pinitized cordierite is commonly preserved, which also records  $S_1$ . The coarse, micaceous alteration products of cordierite also appear to define a crude internal schistosity, which has been shown in samples with unaltered cores to be congruent with  $S_1$ . Similar observations have been noted in schist of the Cooma Complex, Australia, in which "...micaceous intergrowths have mimetically enhanced an included foliation in the cordierite..." (Vernon, 1988, p. 256).

Two textural varieties of andalusite are observed in the rocks: blocky, prismatic andalusite (up to 10 mm) and anhedral-skeletal andalusite. Prismatic andalusite occurs in two of the eight samples. It is commonly partially or totally altered to sericite, obscuring any internal structure. The  $S_2$  matrix schistosity weakly wraps prismatic andalusite porphyroblasts, although some  $S_2$  fabric truncations along porphyroblast margins have also been observed.

The anhedral-skeletal variety of andalusite is found in three samples. It occurs as interstitial grains between cordierite porphyroblasts, as discontinuous skeletal concentrations on the margins of cordierite grains, and as spongy matrix sieves (Fig. 6 and 7). In contrast to the prismatic variety of andalusite, the anhedral-skeletal andalusite overgrows the dominant  $S_2$  fabric. Similar textural associations of andalusite and cordierite have been reported in the Cooma Complex, Australia (Vernon, 1978, 1988) and in the Bugaboo aureole (Pattison et al., 2002).

In most samples, the matrix schistosity is overprinted by randomly oriented chlorite microporphyroblasts (Fig. 4), ascribed to a late retrogressive event, perhaps of the same generation as the muscovite+chlorite replacement of cordierite porphyroblasts. In addition to the above minerals, all the rocks contain plagioclase, quartz, and accessory zircon, monazite, titanite, and ilmenite.

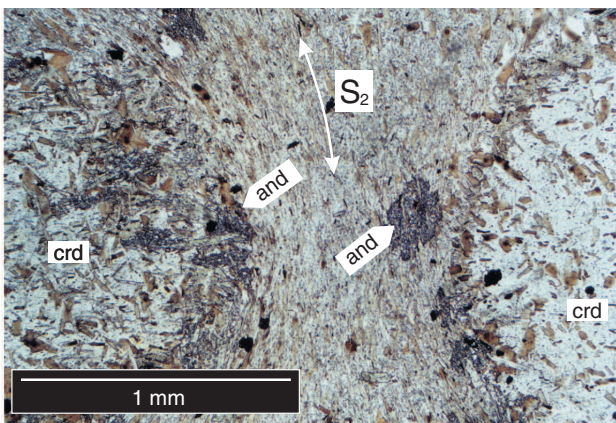


**Figure 6.** Sample A311, plane-polarized light. Post- $D_2$ , skeletal andalusite (and) is growing in the matrix and along cordierite (crd) margins. Cordierite porphyroblasts are unaltered and contain randomly oriented inclusions of biotite in addition to a weak quartz inclusion fabric, running from left to right (not visible).

The muscovite-rich schist near the hinge of the dominant fold structure records two additional, locally developed, late fabrics (*see above*). A steep, south-dipping crenulation cleavage, here defined as  $S_3$ , has quartz-rich and muscovite-rich domains parallel to crenulation axial surfaces and crosscuts the north-northwest-dipping  $S_2$  foliation by approximately  $50^\circ$ . These muscovite-rich pelite units have a second, weaker set of crenulations that are north-plunging. A faint  $S_4$  fabric can be defined for the axial planes of these crenulations of the  $S_2$  surface (Fig. 8).

## ELECTRON MICROPROBE ANALYSIS

Biotite was analyzed from samples A311, A316, and A347 (Fig. 2) to constrain P-T conditions. The analyses were performed with the assistance of R.A. Marr at the University of

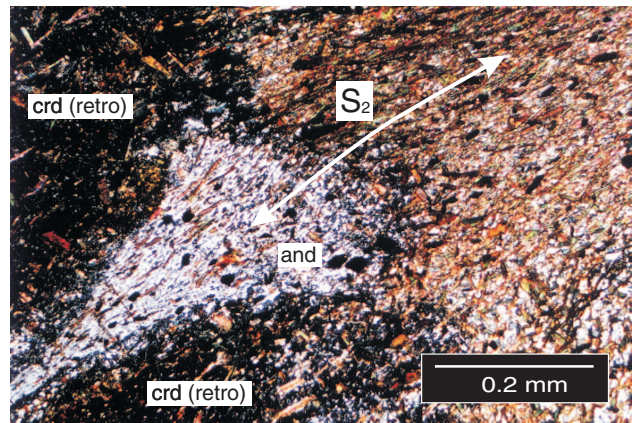


**Figure 7.** Sample A347, cross-polarized light. Post- $D_2$  interstitial andalusite (and) occurs between two retrograded cordierite (crd) grains, overprinting the external schistosity ( $S_2$ ).

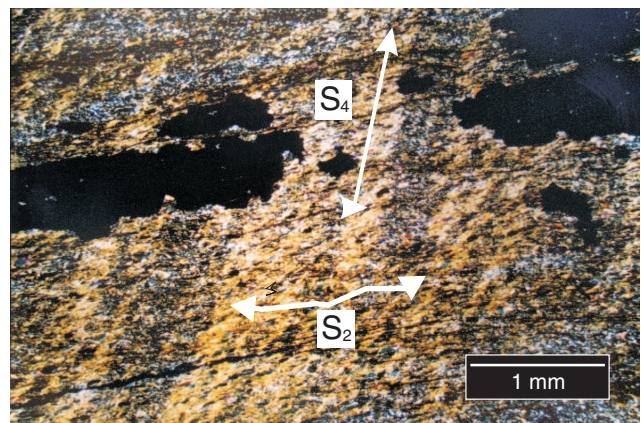


**Figure 8.** Sample A315, cross-polarized light. A weak  $S_4$  fabric results from approximately north-trending crenulations of  $S_2$  in a muscovite-rich schist. The  $S_3$  fabric, much stronger than  $S_4$ , lies approximately in the plane of the image and so is not visible. The black areas are holes in the thin section.



Calgary Laboratory for Electron Microbeam Analysis (UCLEMA) using a JEOL JXA-8200 electron microprobe. Analytical conditions were as follows: voltage = 15 kV, beam current = 20 nA, dwell time = 20 s on peak, 10 s on background. Mineral standards for biotite included orthoclase (Al, Si, K), diopside (Mg), hornblende (Ca), albite (Na), ilmenite (Fe, Ti), and rhodonite (Mn). The results for biotite are shown in Table 1. These values are mean analyses for multiple (2–3) biotite grains, with a range of two to four analyses/grain.

## PHASE EQUILIBRIA

The rocks within the study area have biotite+muscovite+cordierite±andalusite assemblages. These occur upgrade of biotite+muscovite±chlorite occurrences south of the field area, and downgrade of sillimanite+K-feldspar+leucosome occurrences to the north.

The first appearance of cordierite in pelitic rocks arises from the six-phase reaction muscovite + chlorite + quartz = cordierite + biotite + H<sub>2</sub>O (2, Fig. 9a) (reactions are numbered according the scheme in Pattison et al., 2002). Reaction 2 can be modelled in the five-component K<sub>2</sub>O-(MgO or FeO)-Al<sub>2</sub>O<sub>3</sub>-SiO<sub>2</sub>-H<sub>2</sub>O (KFASH or KMASH) system as a univariant equilibrium (Fig. 9a). An analogous chlorite-consuming reaction that introduces andalusite rather than cordierite is muscovite + chlorite = Al<sub>2</sub>SiO<sub>5</sub> + biotite + quartz + H<sub>2</sub>O (4, Fig. 9a).

Upgrade of reactions 2 and 3 (Fig. 9a), andalusite may form at the expense of cordierite through the reaction muscovite + cordierite = biotite + Al<sub>2</sub>SiO<sub>5</sub> + quartz + H<sub>2</sub>O (1, Fig. 9a).

Because the bulk composition of pelite invariably includes both Mg and Fe, the model six-component KFMASH system is a more realistic representation of most natural pelitic assemblages (Fig. 9b). In this system, reactions 1, 2, and 4 become divariant reactions bounded by Fe and Mg end-member reactions. In Figure 9b, an additional univariant equilibrium 8 results, joining the Fe and Mg end-member invariant points of the intersecting 1f-2f-4f and 1m-2m-4m end member equilibria (reactions labeled f and m for Fe and Mg end members, respectively). Reaction 8 is muscovite + chlorite + quartz = cordierite + Al<sub>2</sub>SiO<sub>5</sub> + biotite + H<sub>2</sub>O (8, Fig. 9b). It represents the minimum temperature limit for assemblages containing both cordierite and andalusite.

The upper temperature limit of muscovite+biotite+cordierite±andalusite assemblages is defined by the reaction muscovite + quartz = Al<sub>2</sub>SiO<sub>5</sub> + K-feldspar + H<sub>2</sub>O (5, Fig. 9a, b).

As a result, assemblages in the study area are constrained to lie in the shaded region of Figure 9b, the divariant interval of reaction 1. The presence of andalusite and the absence of sillimanite constrain these assemblages further to part of the divariant interval of reaction 1 that occurs in the andalusite stability field (see below).

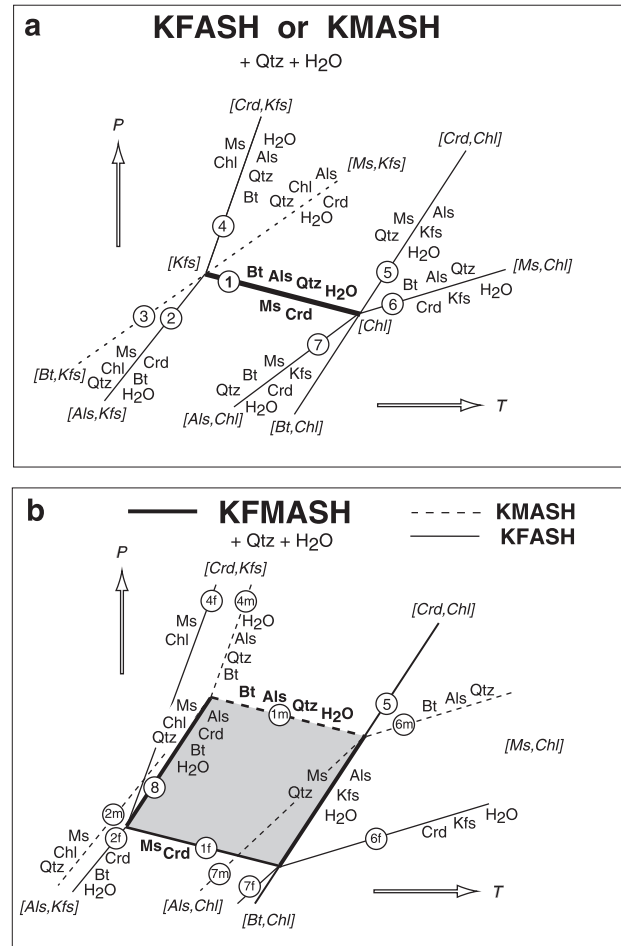


**Figure 9.** Schematic representation of reactions relevant to the study area's pelitic assemblages in the model **a**) KFASH KMASH and **b**) KFMASH systems (after Pattison et al., 2002, Fig. 1). The shaded region in Figure 9b defines the stability limit of muscovite+biotite+cordierite+andalusite assemblages. Als, Al<sub>2</sub>SiO<sub>5</sub>; Bt, biotite; Chl, chlorite; Crd, cordierite; Kfs, K-feldspar; Ms, muscovite; Qtz, quartz

## PRESSURE-TEMPERATURE CONDITIONS

A quantitative representation of the above constraints is provided in the thermodynamically calculated metapelitic petrogenetic grid in Figure 10 (Pattison et al., 2002). The grey shaded region is the divariant interval for reaction 1, contoured with isopleths of Mg/(Mg+Fe) in biotite.

The intersection of reaction 8 with the andalusite = sillimanite reaction restricts the pressure of the muscovite+cordierite+andalusite+biotite assemblages to 4 kbar or less. Because metamorphic assemblages north of the study area contain sillimanite+K-feldspar+leucosome with no andalusite, the metamorphic field gradient likely passes on the

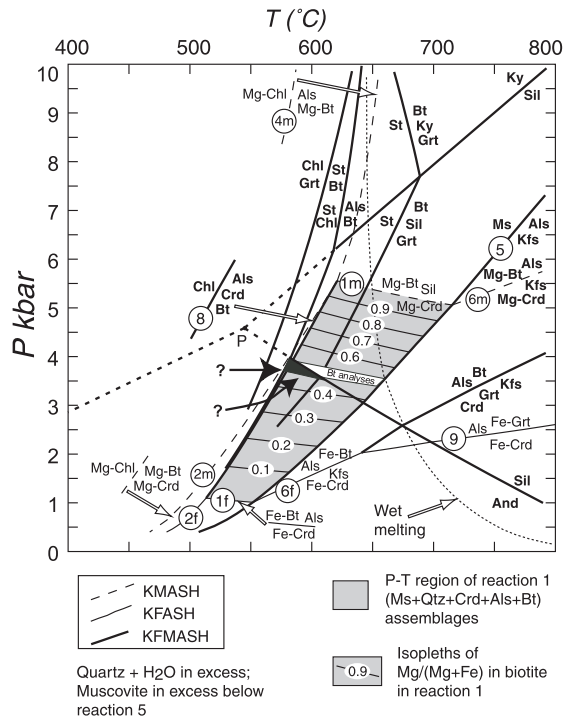


**Figure 10.** Thermodynamically calculated petrogenetic grid for metapelite assuming  $a(H_2O) = 1$  (after Pattison et al., 2002, Fig. 10). The grey shaded region corresponds to the divariant reaction 1m/1f, contoured with isopleths of  $Mg/(Mg+Fe)$  in biotite. The white band labelled 'Bt analyses' represents the measured range of  $Mg/(Mg+Fe)$  in biotite from the study area (0.47–0.53; see Table 1). The intersection of this band with the andalusite stability field gives the black triangle, interpreted to represent peak metamorphic conditions. The black arrows indicate two possible metamorphic field gradients (isobaric and positive  $P$ - $T$  gradient). Als,  $Al_2SiO_5$ ; And, andalusite; Bt, biotite; Chl, chlorite; Crd, cordierite; Fe, iron; Grt, garnet; Kfs, K-feldspar; Ky, Kyanite; Mg, magnesium; Ms, muscovite; Sil, sillimanite; St, staurolite; KMASH,  $K_2O$ -MgO- $Al_2O_3$ - $SiO_2$ - $H_2O$ ; KFASH,  $K_2O$ -FeO- $Al_2O_3$ - $SiO_2$ - $H_2O$ ; KFMASH,  $K_2O$ -MgO-FeO- $Al_2O_3$ - $SiO_2$ - $H_2O$

high-pressure side of the intersection of the univariant equilibria andalusite = sillimanite and muscovite + quartz =  $Al_2SiO_5$  + K-feldspar +  $H_2O$  (5, Fig. 10), giving a minimum pressure of 3 kbar. Therefore, peak  $P$ - $T$  conditions lie in the shaded region in Figure 10 between isopleths of  $Mg/(Mg+Fe)$  in biotite of about 0.35 to 0.55.

This inference was tested by analyzing biotite from three samples (localities shown in Fig. 2), the results of which are given in Table 1. Values of  $Mg/(Mg+Fe)$  range between 0.47 and 0.53, consistent with, but at the high-pressure end, of the inferred range. The intersection of this band of isopleths with the andalusite stability field (Fig. 10) yields a tightly constrained  $P$ - $T$  interval of 3.5 to 4.0 kbar and 570° to 600°C,

although a realistic assessment of uncertainties on the position of the calculated equilibria in Figure 10 would broaden this interval by at least  $\pm 25^\circ C$  and  $\pm 0.5$  kbar. In addition, the isopleths in Figure 10 were calculated assuming the Pattison (1992) triple point. If the Holdaway (1971) triple point is used instead, the isopleths and all attendant pressure estimates fall by about 1 kbar (see Pattison et al., 2002, Fig. 10c).

## PRESSURE-TEMPERATURE-DEFORMATION-TIME PATH

A pressure-temperature-deformation-time path was constructed for the study area by combining microtextural observations on the relative timing of fabric development and porphyroblast growth with the thermodynamically calculated phase diagram (Fig. 10). Figure 11 is a summary of the inferred path, the details of which are discussed below.

### Early deformation ( $D_1$ )

The earliest recognizable tectonic microstructure ( $S_1$ ) is represented by the internal schistosity in cordierite porphyroblasts. This event may correspond to  $D_{1P}$ , which gave rise to structural repetitions of the Piling Group stratigraphy (Corrigan et al., 2001; St-Onge et al., 2001a, b, c, d, 2002a, b, c; Scott et al., 2002).

### Cordierite paragenesis

The growth of cordierite clearly postdates  $D_1$  due to the incorporation of  $S_1$ . Assuming the presence of chlorite in lower grade protoliths, the growth of cordierite can be attributed to the reaction muscovite + chlorite + quartz = cordierite + biotite + vapour (2m/2f, Fig. 10). At 3 to 4 kbar, the temperature of this reaction is 550° to 570°C.

### Biotite paragenesis

Biotite occurs as a common matrix mineral, as inclusions in unaltered cordierite porphyroblasts, and more rarely as intergrowths in altered cordierite grains. Apart from the alteration-related variety, it occurs as irregular, randomly oriented grains whose distribution, grain size, and texture are largely the same whether in the matrix or as inclusions in cordierite. Electron-microprobe data indicate no obvious variations in biotite composition that can be related to its morphology or textural context (e.g. sample A311, Table 1).

Although some biotite must have been produced along with cordierite in reaction 2m/2f, it is too abundant in the rocks for reaction 2m/2f alone to account for all of it. Where biotite occurs as inclusions in unaltered cordierite porphyroblasts, the grain size is much larger than that of  $S_1$ -defining quartz inclusions. It therefore seems likely that most biotite grew after  $D_1$ , but before cordierite growth, an inference supported by biotite-rich, cordierite-absent assemblages at lower metamorphic grade south of the study area. The development of early biotite in the schist of the study area is therefore

**Table 1.** Results from mean biotite analyses.

OXIDE	A311		A316 matrix (3 grains)	A347 matrix (2 grains)
	matrix (3 grains)	in cordierite (3 grains)		
SiO <sub>2</sub>	35.21	36.02	35.63	35.56
Al <sub>2</sub> O <sub>3</sub>	20.83	20.81	19.96	20.82
TiO <sub>2</sub>	1.38	0.87	1.44	1.17
FeO	19.18	19.91	19.45	17.73
MgO	9.75	10.01	10.05	11.20
MnO	0.10	0.09	0.12	0.11
CaO	0.00	0.00	0.03	0.00
Na <sub>2</sub> O	0.24	0.22	0.14	0.26
K <sub>2</sub> O	8.88	9.03	8.53	8.73
Sum	95.57	96.96	95.34	95.58
CATIONS (O = 22)	A311		A316 matrix	A347 matrix
	matrix	in cordierite		
Si	5.31	5.36	5.38	5.32
Al	3.70	3.65	3.55	3.67
Ti	0.16	0.10	0.16	0.13
Fe	2.42	2.48	2.46	2.22
Mg	2.19	2.22	2.26	2.50
Mn	0.01	0.01	0.02	0.01
Ca	0.00	0.00	0.00	0.00
Na	0.07	0.06	0.04	0.08
K	1.71	1.72	1.64	1.66
Sum	15.57	15.60	15.52	15.59
Mg/(Mg+Fe)	0.475	0.473	0.480	0.530

ascribed to a reaction such as phengitic muscovite + chlorite = less phengitic muscovite + biotite + quartz + H<sub>2</sub> (Pattison, 1987).

### Second deformation event (D<sub>2</sub>)

The penetrative, north-northwest-dipping fabric (S<sub>2</sub>) clearly wraps cordierite porphyroblasts and therefore postdates cordierite growth. In some samples, the S<sub>2</sub> fabric is truncated against the strain-shadow side of cordierite porphyroblasts, suggesting that the onset of D<sub>2</sub> may have overlapped with the growth of cordierite. The D<sub>2</sub> event is likely equivalent to the regional D<sub>2p</sub> event interpreted for the Central Baffin Project map area (Corrigan et al., 2001; Scott et al., 2002).

Although the S<sub>2</sub> fabric wraps the cordierite porphyroblasts and the long axes of the egg-shaped porphyroblasts lie at various angles with respect to S<sub>2</sub>, the internal S<sub>1</sub> fabric within the cordierite porphyroblasts is largely of the same orientation for all porphyroblasts. This observation suggests that the matrix fabric was re-orientated around the cordierite porphyroblasts during D<sub>2</sub> without inducing significant rotation of the porphyroblasts (see Bell, 1985; Vernon, 1989). Whether this observation pertains to all the rocks examined cannot be determined because of the commonly severe retrogression of cordierite.

### Prismatic andalusite paragenesis

Blocky prismatic andalusite porphyroblasts are partially wrapped by S<sub>2</sub>, but not to the extent of most cordierite porphyroblasts. This variety of andalusite may therefore have grown during the late stages of D<sub>2</sub>. Because this morphology

of andalusite is typically altered to sericite, possible S<sub>1</sub>–S<sub>2</sub> relationships have been obliterated. This early form of andalusite may have been formed along with some relatively late cordierite by the reaction muscovite + chlorite + quartz = cordierite + andalusite + biotite + vapour (8, Fig. 10).

Reaction 8 occurs at a slightly higher temperature than the divariant interval represented by the cordierite-forming reaction 2m/2f and can only proceed if chlorite is not consumed in reaction 2m/2f. Although chlorite is common in the schist, all of it appears to be secondary.

### Anhedral–skeletal andalusite paragenesis and relationship to D<sub>2</sub>

The anhedral–skeletal variety of andalusite (interstitial grains between cordierite, skeletal growths on cordierite, and isolated matrix sieves) overprints the external S<sub>2</sub> fabric as revealed by inclusion trails of quartz and biotite that are continuous with S<sub>2</sub> (Fig. 8). It therefore postdates D<sub>2</sub>. It is interpreted to have formed upgrade of reaction 8 through the reaction cordierite + muscovite = andalusite + biotite + quartz + vapour (1m/1f, Fig. 10).

Evidence for the instability of cordierite is provided by the skeletal growth of andalusite on the margins of cordierite porphyroblasts.

Formation of late andalusite by reaction 1m/1f implies that the P-T path involved isobaric heating or a combination of heating and pressure increase (see Fig. 10). Although the latter might seem to be more likely given that the rocks underwent compressional orogenesis involving thrusting and folding in D<sub>1</sub> and D<sub>2</sub>, the lack of S<sub>2</sub> deflection around this late variety of andalusite suggests static growth and, consequently, isobaric heating. Regardless of the exact P-T path, the temperature of formation of this late andalusite is fairly well constrained to 580° to 600°C (i.e. above reaction 8 but below the andalusite = sillimanite reaction; see Fig. 10). This represents the peak temperature reached by the rocks in the study area. Given that the late variety of andalusite grew after S<sub>2</sub> and cordierite grew largely before S<sub>2</sub>, the temperature at which the S<sub>2</sub> formed in the study area is tightly constrained to 560° to 600°C.

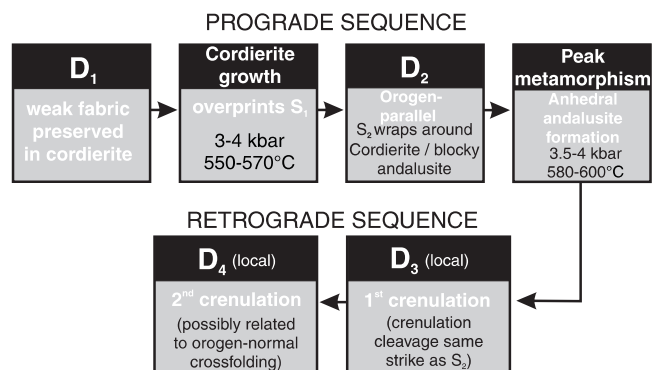


**Figure 11.** Summary of the relative chronology of deformation events and metamorphic phase growth episodes.

### Late deformation ( $D_3$ and $D_4$ )

Evidence for the third deformation event ( $D_3$ ) is recorded locally in muscovite-rich schist as a crenulation cleavage ( $S_3$ ) crosscutting the north-northwest-dipping  $S_2$  fabric (see above). The  $D_3$  event, although approximately east-trending and therefore orogen-parallel, is apparently unrelated to  $D_2$  and has no manifestation in regional structures.

Intersecting crenulations are evidence for a still later deformation event ( $D_4$ ) in the same muscovite-rich schist. These north-plunging crenulations may be related to orogen-perpendicular crossfolding ( $D_{3P}$  in the scheme of Corrigan et al., 2001; Scott et al., 2002). If so, they display the only microstructural evidence for this late crossfolding event (Fig. 8). There are no P-T constraints on the development of the late crenulation fabrics ( $D_3$  and  $D_4$ ), so the shape of the retrograde P-T path is unknown.

### IMPLICATIONS FOR METAMORPHISM OF THE FOXE FOLD BELT

Peak P-T conditions of approximately 600°C at 3 to 4 kbar (Fig. 10) imply an anomalously high geothermal gradient of 50° to 60°C/km, which becomes even more extreme if a lower pressure triple point is considered (see Pattison et al., 2002, Fig. 10c). Such temperatures are well above what can be generated in models of orogenic thickening using standard mantle heat-flow and radioactive heat-generation parameters (e.g. England and Thompson, 1984; Jamieson et al., 2002). Whereas an obvious potential source of additional heat comes from the emplacement of magmas, no evidence was found for magmatic activity in the vicinity of the study area. Rather, the microtextures in the rocks seem to indicate that prograde metamorphism occurred during the later stages of orogenic thickening. This may suggest that radioactive heat generation was considerably higher in these Proterozoic turbiditic rocks than in their present-day equivalents, consistent with a secular decrease in radioactivity through geological time (Chacko, 1997).

### ACKNOWLEDGMENTS

Marc St-Onge, David Scott, and David Corrigan are warmly thanked for ably leading the Central Baffin Project and encouraging student involvement. The GSC, the Canada-Nunavut Geoscience Office, the Polar Continental Shelf Project, and the University of Calgary are gratefully acknowledged for financial and logistical support. The remainder of the Baffin crew are thanked for their companionship and insight. Electron microprobe analyses were performed with the assistance of Robert Marr at the University of Calgary Laboratory for Electron Microbeam Analysis (UCLEMA). Marc St-Onge, David Scott, and Ed Ghent are thanked for suggesting improvements to this manuscript or to the original B.Sc. thesis from which it was derived.

### REFERENCES

- Bell, T.H.**  
1985: Deformation partitioning and porphyroblast rotation in metamorphic rocks: a radical reinterpretation; *Journal of Metamorphic Geology*, v. 3, p. 109–118.
- Chacko, T.**  
1997: Ultra-high temperature metamorphism at Pelican Rapids, Taltson Magmatic Zone, NE Alberta: possible implications for early Proterozoic collisional orogens; *Geological Association of Canada—Mineralogical Association of Canada, Abstracts*, v. 22, p. A24.
- Corrigan, D., Scott, D.J., and St-Onge, M.R.**  
2001: Geology of the northern margin of the Trans-Hudson Orogen (Foxy Fold Belt), central Baffin Island, Nunavut; *Geological Survey of Canada, Current Research 2001-C23*, p. 1–29.
- England, P.C. and Thompson, A.B.**  
1984: Pressure-temperature-time paths of regional metamorphism. I. Heat transfer during the evolution of regions of thickened continental crust; *Journal of Petrology*, v. 25, p. 894–928.
- Hoffman, P.H.**  
1988: United plates of America, the birth of a craton: Early Proterozoic assembly and growth of Laurentia; *Annual Reviews of Earth and Planetary Sciences*, v. 16, p. 543–603.
- Holdaway, M.J.**  
1971: Stability of andalusite and the aluminum silicate phase diagram; *American Journal of Science*, v. 271, p. 97–131.
- Jamieson, R.A., Beaumont, C., Nguyen, M.H., and Lee, B.**  
2002: Interaction of metamorphism, deformation, and exhumation in large convergent orogens; *Journal of Metamorphic Geology*, v. 20, p. 9–24.
- Passchier, C.W. and Trouw, R.A.J.**  
1996: *Microtectonics*; Springer-Verlag, Berlin, Germany, 283 p.
- Pattison, D.R.M.**  
1987: Variations in Mg/(Mg + Fe), F, and (Fe,Mg)Si = 2Al in pelitic minerals in the Ballachulish thermal aureole, Scotland; *American Mineralogist*, v. 72, p. 255–272.  
1992: Stability of andalusite and sillimanite and the  $Al_2SiO_5$  triple point; constraints from the Ballachulish aureole, Scotland; *Journal of Geology*, v. 100, p. 423–446.
- Pattison, D.R.M. and Tracy, R.J.**  
1991: Phase equilibria and thermobarometry of metapelites; in *Contact Metamorphism, Reviews in Mineralogy*, (ed.) D.M. Kerrick; Mineralogical Society of America, v. 26, p. 105–206.
- Pattison, D.R.M., Spear, F.S., Debuhr, C.L., Cheney, J.T., and Guidotti, C.V.**  
2002: Thermodynamic modelling of the reaction muscovite + cordierite →  $Al_2SiO_5$  + biotite + quartz +  $H_2O$ : constraints from natural assemblages and implications for the metapelitic petrogenetic grid; *Journal of Metamorphic Geology*, v. 20, p. 99–118.
- Scott, D.J., St-Onge, M.R., and Corrigan, D.**  
2002: Geology of the Paleoproterozoic Piling Group and underlying Archean gneiss, central Baffin Island, Nunavut; *Geological Survey of Canada, Current Research 2002-C17*, 10 p.
- St-Onge, M.R., Scott, D.J., and Corrigan, D.**  
2001a: Geology, MacDonald River, Nunavut; *Geological Survey of Canada, Open File 3958*, scale 1:100 000.  
2001b: Geology, Flint Lake, Nunavut; *Geological Survey of Canada, Open File 3959*, scale 1:100 000.  
2001c: Geology, Nadluardjuk Lake, Nunavut; *Geological Survey of Canada, Open File 3960*, scale 1:100 000.  
2001d: Geology, Wordie Bay, Nunavut; *Geological Survey of Canada, Open File 3961*, scale 1:100 000.  
2002a: Geology, north Tweedsmuir Island, Nunavut; *Geological Survey of Canada, Open File 4199*, scale 1:100 000.  
2002b: Geology, Straits Bay, Nunavut; *Geological Survey of Canada, Open File 4200*, scale 1:100 000.  
2002c: Geology, Dewar Lakes, Nunavut; *Geological Survey of Canada, Open File 4201*, scale 1:100 000.

**Vernon, R.H.**

- 1978: Pseudomorphous replacement of cordierite by symplectic intergrowths of andalusite, biotite, and quartz; *Lithos*, v. 11, p. 283–289.
- 1988: Sequential growth of cordierite and andalusite porphyroblasts, Cooma Complex, Australia: microstructural evidence of a prograde reaction; *Journal of Metamorphic Geology*, v. 6, p. 255–269.
- 1989: Porphyroblast-matrix microstructural relationships: recent approaches and problems; *in* *Evolution of Metamorphic Belts*, (ed.) J.S. Daly, R.A. Cliff, and B.W.D. Yardley; Geological Society Special Publication, v. 43, p. 83–102.

**Wodicka, N., St-Onge, M.R., Scott, D.J., and Corrigan, D.**

- 2002: Preliminary report on the U-Pb geochronology of the northern margin of the Trans-Hudson Orogen, central Baffin Island, Nunavut; Geological Survey of Canada, Current Research 2002-F7; Radiogenic Age and Isotopic Studies: Report 15, 12 p.

---

Geological Survey of Canada Project PS1006